

F-CAM: Full Resolution CAM via Guided Parametric Upscaling

Soufiane Belharbi¹, Aydin Sarraf³, Marco Pedersoli¹, Ismail Ben Ayed¹, Luke McCaffrey², and Eric Granger¹

¹ LIVIA, Dept. of Systems Engineering, École de technologie supérieure, Montreal, Canada

² Goodman Cancer Research Centre, Dept. of Oncology, McGill University, Montreal, Canada

³ Ericsson, Montreal, Canada

soufiane.belharbi.1@ens.etsmtl.ca, luke.mccaffrey@mcgill.ca

{ismail.benayed, eric.granger, marco.pedersoli}@etsmtl.ca

aydin.sarraf@ericsson.com

ABSTRACT

Class Activation Mapping (CAM) methods have recently gained much attention for weakly-supervised object localization (WSOL) tasks, allowing for CNN visualization and interpretation without training on fully annotated image datasets. CAM methods are typically integrated within off-the-shelf CNN backbones, such as ResNet50. Due to convolution and downsampling/pooling operations, these backbones yield low resolution CAMs with a down-scaling factor of up to 32, making accurate localization more difficult. Interpolation is required to restore a full size CAMs, but without considering the statistical properties of the objects, leading to activations with inconsistent boundaries and inaccurate localizations. As an alternative, we introduce a generic method for parametric upscaling of CAMs that allows constructing accurate full resolution CAMs (F-CAMs). In particular, we propose a trainable decoding architecture that can be connected to any CNN classifier to produce more accurate CAMs. Given an original (low resolution) CAM, foreground and background pixels are randomly sampled for fine-tuning the decoder. Additional priors such as image statistics, and size constraints are also considered to expand and refine object boundaries. Extensive experiments¹ using three CNN backbones and six WSOL baselines on the CUB-200-2011 and OpenImages datasets, indicate that our F-CAM method yields a significant improvement in CAM localization accuracy. F-CAM performance is competitive with state-of-art WSOL methods, yet it requires fewer computational resources during inference.

Keywords: Convolutional Neural Networks, Weakly-Supervised Object Localization, Class Activation Mapping, Interpretability.

1 Introduction

Deep learning (DL) models, and in particular CNNs, provide state-of-the-art performance in many visual recognition applications, such as image classification and object detection. However, they remain complex models that typically require

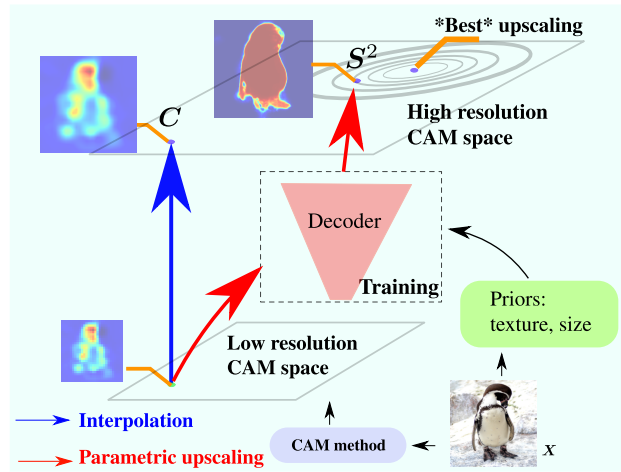


Figure 1: An illustration of the differences between interpolation and trainable parametric upscaling with priors. C is the interpolated CAM, and S^2 is the F-CAM produced using our proposed trainable decoder architecture.

supervised end-to-end training on large annotated datasets. Weakly supervised learning (WSL) has recently emerged as an approach to mitigate the cost and burden of annotating large datasets, by exploiting data with limited or coarse labels [58]. In particular, WSL is largely beneficial in object localization to avoid the costly annotation such as bounding boxes. Indeed, weakly-supervised object localization (WSOL) methods rely on image-level classification labels, which are easy to acquire.

Authors in [57] introduce Class Activation Maps (CAMs), and show that spatial feature maps of standard deep models trained using only image class already provide rich spatial information that could be used for object localization without additional supervision. CAMs allow highlighting important regions of an input image linked to the CNN’s predictions. Because the model is trained for classification task using global label only, CAMs tend to activate only on small discriminative regions while missing large part of the body. Since then, several extensions have been proposed to alleviate this issue. In particular, WSOL methods based on data

¹Public code: <https://github.com/sbelharbi/fcam-wsol>.

enhancement [9, 34, 45, 51, 53] aim to push the model to be less dependent on most discriminative regions and seek additional regions. For instance, [34] divide the input image into patches and only few of them are used during training forcing the model to look for variant discriminative regions. Due this random information suppression in the input image, model could easily confuse objects and background leading to high false positives due to the insufficient discriminative regions. Other methods consider improving the feature maps [18, 29, 44, 46, 47, 48, 52, 54]. For instance, [46] consider using dilated convolution to adapt to objects with different sizes. [52] argue that WSOL task needs to be divided into object classification and class-agnostic localization. The latter generates noisy pseudo-annotation, then perform bounding box regression with them for an accurate localization without interference with classification task. Authors in [46] enhance the features by considering shallow features of deep models yielding new state-of-the-art performance in WSOL task, and demonstrating the benefit of low features for object localization. All these methods are model-dependent. Using them requires training a model following their design. Different from these families, other WSOL methods are proposed to be generic, model-independent, and allow to interrogate the localization of target label over a pretrained classifier. Such branch of methods include Gradient-weighted Class Activation Mapping (Grad-CAM), Grad-CAM++, Ablation-CAM and Axiom-based Grad-CAM [12, 19, 28].

All these methods are typically applied with an off-the-shelf CNN backbone for feature extraction, such as Inception and ResNet. Due to multiple strided convolution and pooling operations, these backbones yield low resolution CAMs with downscale factor up to 32^2 . In this case, each pixel in the CAM covers a patch of 32×32 pixels in the input image making the CAM vulnerable to localization inaccuracies. Interpolation is often used to generate full size CAMs, yet such operation does not take in consideration statistical properties of objects or its shape. This leads to bloby localization with inaccurate boundaries (see Fig.3, 4). Moreover, CAMs lack explicitly modeling the background. This plays a central role in increasing false positives/negative where for instance parts of the background could be considered as object [31]. In addition, in WSOL task, using only global label as a supervisory signal without having access to pixel-level is considered an ill-posed problem [8, 42] that may lead to sub-optimal solutions. The issue of low resolution CAMs is largely overlooked in the literature. Dilated residual networks (DRN) [50] addressed explicitly this issue. Compared to ResNet family [14] that can produce a map of 7×7 for an input of 224×224 , the DRN can produce a map of size 28×28 . Despite this improvement, the CAMs are still low resolution with downscale factor of 8.

²In practice, it is common to modify the convolution stride and maxpooling layers to reduce the downsampling factor.

In this paper, we aim to improve the resolution and localization accuracy of CAMs. As an alternative to interpolation, we propose to equip a classifier employed for WSOL with a *parametric* decoder architecture that is trained to gradually upscale the resolution of feature maps, and construct a full resolution CAM (Fig.2). We explicitly model the foreground and background using the decoder, allowing for robust localization. The decoder outputs two activation maps, one for the foreground and other for the background with the same size as the input image. Using a decoder such as in Fig.2 which has the U-Net form [30] is mainly motivated by deep image prior with its successful application to super-resolution task [40] and other tasks including denoising, and inpainting. Fig.1 shows the intuition of our method and its connection to deep image prior [40]. Authors in [40] show that such convolutional architectures with skip connections capture a large part of low-level image statistics. Such low details turn out to play a critical part in improving localization such as it was demonstrated in the recent state-of-the-art method in WSOL task [44]. This confirms that exploiting fine-grained details in deep networks is a promising direction to improve localization accuracy. In contrast to the work in [40] in which

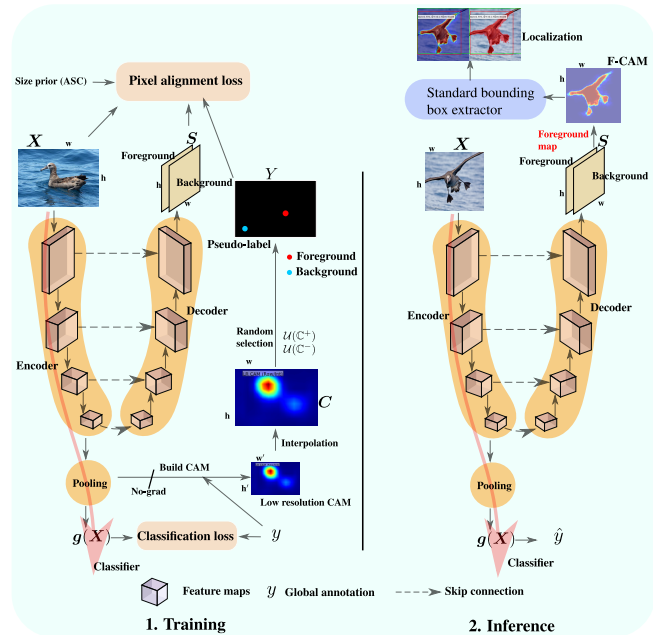


Figure 2: Our Proposal. *Left*: training. *Right*: inference.

a transductive learning setup is used for super-resolution task without supervision, we consider an inductive learning using guidance allowing fast inference but *without additional supervision*. In particular, we propose to use local and global constraints to train the decoder. Local constraints entails pixel alignment with pseudo-annotation harvested from the CAMs of a WSOL classifier. In addition, consistency loss such as conditional random field (CRF) is used to align the activations

with the object boundaries by exploiting statistical properties of the image such as color and local proximity between pixels. We use an additional global constraint to recover complete part of the object using size prior.

Our main contributions are summarized below: **1)** We propose a simple yet efficient alternative to interpolation to improve the quality of CAMs. Given a CNN classifier employed for WSOL, we propose to integrate a decoder architecture for parametric upscaling of CAMs. It leverages low/top-level features from the classifier to map original (low resolution) CAMs to full-resolution CAMs (F-CAMs) that can produce accurate localizations. In addition, the decoder explicitly models foreground and background. **2)** Training of the decoder is performed using loss terms that ensure the accuracy, consistency, and completeness of F-CAMs, using only the global image-class annotation provided for supervision. We exploit low resolution CAMs in addition to image statistics and object size priors for training the decoder. Our method is generic, and can be combined with any WSOL method with a classifier. It aims solely to improve the CAM quality and therefore improve the localization performance without altering the classification performance. **3)** Following the experimental WSOL protocol described in [8], we compare F-CAM against several baseline methods, including CAM [57], GradCAM [32], GradCam++ [7], Smooth-GradCAM++ [25], XGradCAM [12], LayerCAM [15], on two benchmark datasets for WSOL, CUB-200-2011 [41] and OpenImages [5, 8]. Results indicate that F-CAM can provide significant improvements in localization for these baselines. In addition, F-CAMs produced with our method has better properties, like less sensitivity to threshold values, which is also a bottleneck in WSOL tasks. The enhanced results made these WSOL baselines competitive with recent WSOL state-of-the-art methods. **4)** Finally, we also provide ablation studies and a complexity analysis to characterize our method. The inference time obtained with F-CAM is lower than average standard CAM methods.

2 Proposed approach

Notation. Consider a training set $\mathbb{D} = \{(\mathbf{X}, y)_i\}_{i=1}^N$ where $\mathbf{X} : \Omega \subset \mathbb{R}^2$ is an image with its global label $y \in \{1, \dots, K\}$ with K possible classes. Our model is composed of a classifier g to perform classification, and a decoder f to output two activation maps, one for the foreground and the other for background, used for object localization. The classifier is composed of: (a) a feature encoder for building features, (b) and a pooling head to compute classification scores. For simplicity, θ refers to the parameters of entire model (see Fig. 2). $g(\mathbf{X}) \in [0, 1]^K$ denotes the per-class classification probabilities where $g(\mathbf{X})[k] = \Pr(k|\mathbf{X})$. The softmax activation maps generated by the decoder is denoted $\mathbf{S} = f(\mathbf{X}) \in [0, 1]^{|\Omega| \times 2}$ where $\mathbf{S}^1, \mathbf{S}^2$ are the background and foreground maps, re-

spectively. The map \mathbf{S}^2 is class-agnostic, meaning it can hold the activation of any class y . The classifier yields an interpolated CAM, referred to as \mathbf{C} , of the target y with the same resolution as the image. $\mathbf{S}_p \in [0, 1]^2$ is a row of the matrix \mathbf{S} corresponding to a point $p \in \Omega$.

Generation of sampling regions (SRs). In order to guide the fine-tuning of the decoder, we employ local information at pixel level as a supervisory signal. WSOL task aims to produce a bounding box with foreground inside and the left-over is considered background. Similarly, to decide a pixel state (foreground or background), we rely on the activate magnitude in \mathbf{C} . Because such activations hint the presence or absence of an object, we can fairly assume that pixels with high activations as more likely to be foreground, while lower activations are background [11]. We note $\mathbb{C}^+, \mathbb{C}^-$ as foreground and background regions, respectively. We estimate both regions as follows,

$$\mathbb{C}^+ = TOP^+(\mathbf{C}), \quad \mathbb{C}^- = TOP^-(\mathbf{C}), \quad (1)$$

where $TOP^+(\mathbf{C})$ is the set of top³ pixels in \mathbf{C} , which is ordered from high to low activation, and $TOP^-(\mathbf{C})$ is the set of top pixels in \mathbf{C} which is ordered from low to high activation. Without adding additional hyper-parameters, $TOP^+(\mathbf{C})$ takes all pixels in \mathbf{C} with activation above Otsu [26] threshold obtained over \mathbf{C} . $TOP^-(\mathbf{C})$ sorts activations in \mathbf{C} from low to high and takes the $n\%$ of top pixels. Pixels in \mathbb{C}^+ are assigned hard pseudo-label $\{1\}$ for foreground and pixels in \mathbb{C}^- are assigned 0 for background.

The estimated sampling regions $\mathbb{C}^+, \mathbb{C}^-$ are uncertain and can contain incorrect labels. Because standard CAMs are often bloby, the foreground \mathbb{C}^+ could contain background regions. Similarly, \mathbb{C}^- is expected to hold background pixels but also parts of the object since standard CAMs are incomplete. Due to this uncertainty and noise in labels, we avoid fitting the model directly on $\mathbb{C}^+, \mathbb{C}^-$ at once. Instead, we randomly select only few pixels at each training iteration, while dropping the remaining pixels [34, 36]. To this end, we define a stochastic set of pixels randomly selected from foreground and background as,

$$\Omega' = \mathcal{U}(\mathbb{C}^+) \cup \mathcal{U}(\mathbb{C}^-), \quad (2)$$

where $\mathcal{U}(\mathbb{C}^+)$ is a uniformly sampled pixel from the set \mathbb{C}^+ . Y denotes the *partially* pseudo-labeled mask for the sample \mathbf{X} , where $Y_p \in \{0, 1, nan\}^2$ with labels 0 for background, 1 for foreground, and *nan* for unknown label. This stochastic sampling aims to avoid overfitting on $\mathbb{C}^+, \mathbb{C}^-$ since they are uncertain.

Overall training loss. Our training loss combines two main terms: a standard classification loss, and our proposed loss

³In this context, the top n elements of a list ordered from value a toward b are the initial n elements of the list.

for fine-tuning the decoder named *pixel alignment loss*. This loss entails local (*i.e.*, pixel level) and global terms. The local term aims at aligning the output activations \mathbf{S} with the pseudo-labeled pixels selected in Ω' using partial cross-entropy \mathbf{H} . To promote the consistency in activations, and align them with the object boundaries, we exploit statistical properties of the image such as the color, and also pixel proximity allowing nearby pixels with similar color to be assigned similar state (*i.e.*, foreground or background). To this end, we include the conditional random field loss (CRF) [38], \mathcal{R} .

Since CAMs often highlight only small discriminative regions, they are mostly concentrated in the same neighborhood in the form of a blob. This could prevent the expansion of foreground guided by CRF loss, in particular for objects with variable textures. To circumvent this issue, the activations of the foreground are explicitly pushed to expand through a global constraint. In particular, we consider the absolute size constraint (ASC) [4] over the foreground and background. We do not assume whether the background is larger than the foreground [27] nor the opposite. The ASC loss expands the sizes to be large, provided counter terms to control any arbitrary growth of size. In this work, partial cross entropy, and CRF control the growth of the size to be consistent and avoid degenerate sizes. It is formulated through inequality constraints that are solved via standard log-barrier method [6]. Our overall training loss is formulated as,

$$\begin{aligned} \min_{\theta} \quad & -\log(g(\mathbf{X})[y]) + \alpha \sum_{p \in \Omega'} \mathbf{H}(Y_p, \mathbf{S}_p) + \lambda \mathcal{R}(\mathbf{S}, \mathbf{X}), \\ \text{s.t.} \quad & \sum \mathbf{S}^r \geq 0, \quad r \in \{1, 2\}, \end{aligned} \quad (3)$$

where $\mathbf{H}(Y_p, \mathbf{S}_p) = -\sum_t Y_p^t \log(\mathbf{S}_p^t)$ is the cross-entropy between the \mathbf{S}_p and the pseudo-label mask Y_p at pixel p , and α, λ are balancing coefficients.

It is important to note that training with our method (Eq.3) does not require any additional supervision beside the already provided global annotation y of the class label. This label is used to build the CAM of the target as presented in Fig.2. Another important aspect is the semantic meaning of the foreground in \mathbf{S}^2 . Since \mathbb{C}^+ holds pixels that are assumed foreground estimated from the CAM \mathbf{C} of the true label y , the foreground predicted in \mathbf{S}^2 is expected to be consistent with the global annotation y of the image. In addition, localization using our CAM is similar to standard methods (Fig.2, *inference*).

3 Results and discussion

3.1 Experimental methodology:

Datasets. To evaluate our method, two datasets from [8] are adopted: CUB-200-2011 (CUB) [41] and OpenImages

[5, 8]. CUB contains 200 categories of birds with 5,994 training images and 5,794 testing images. In addition, 1000 extra images annotated in [8] are used as a validation set for model and hyper-parameters selection. OpenImages contains 37,319 images of 100 classes. 29,819 samples are used for training, while 2,500 samples are used for validation. The 5,000 remaining images are used for test. Different from CUB, OpenImages WSOL dataset provides pixel annotation of objects instead of bounding boxes for a fine localization. We follow protocol in [8] for both datasets.

Evaluation metrics. Following [8], we report 5 localization metrics and one classification metric. For localization, we report MaxBoxAcc (also known as CorLoc [10], and GT-known [34]): fraction of images for which the predicted bounding box has more than $\sigma = 50\%$ IoU with the ground truth, independently from classification prediction, MaxBoxAccV2 : the same as MaxBoxAcc but averaged over three sizes $\sigma \in \{30\%, 50\%, 70\%\}$, top-1 localization accuracy: fraction of images with the correct class prediction and more than $\sigma = 50\%$ IoU with the ground truth box, and top-5 localization accuracy: fraction of images with class label belonging to the top-5 predictions and more than $\sigma = 50\%$ IoU. With OpenImages, we report the P@AP metric proposed in [8] which computes the area under the precision-recall curve. As in [8], the CAM's threshold is marginalized over the interval $\tau \in [0, 1]$ with a step of .001.

Implementation details. In all experiments, we follow the same protocol as [8] including backbones, training epochs (50 for CUB and 10 for OpenImages), and batch size of 32. We validated our method over three backbones VGG16 [33], InceptionV3 [37], and ResNet50 [14]. In Eq.3, the hyper-parameter λ for the CRF is set to the same value as in [38] which is $2e^{-9}$. For log-barrier optimization, hyper-parameter t is set to the same value as in [2, 16]. It is initialized to 1, and increased by a factor of 1.01 each epoch with a maximum value of 10. α is searched in $\{1., .1\}$ through validation. We find that strong values do not harm the performance. In all experiments with our method, we used a learning rate of .01 using SGD for optimization. Similar to [8], images are resized to 256×256 , then randomly cropped to 224×224 for training. n^- is chosen on the validation set from the set $[.1, .7]$ with a step of .1.

Baseline models. To validate our F-CAM method, we compare with recent WSOL methods, including: CAM [57], HaS [34], ACoL [53], SPG [54], ADL [9], CutMix [51], CSTN [22], TS-CAM [13], MEIL [21], DANet [47], SPOL [44], ICL [17], NL-CCAM [49], I²C [55], RCAM [56], GC-Net [20], ADL-TAP [1], GradCAM [32], GradCam++ [7], Smooth-GradCAM++ [25], XGradCAM [12], LayerCAM [15]. For CAM, HaS, ACoL, SPG, ADL, and CutMix, we present the results reported in [8]. For GradCAM, GradCam++, Smooth-GradCAM, XGradcam, and Lay-

erCAM, we have reproduced their results. We also reproduce for CAM, and name its results as CAM* to distinguish it from CAM’s results in [8]. For the rest of the methods, we present what was reported in their original papers. Missing values are presented here by —. [8] provide results using few-shot learning (FSL) where few fully supervised samples are used to training the model. A simple baseline is also provided in [8] which is a center-Gaussian baseline. It generates isotropic Gaussian score maps centered at the image. This represents a lower bound performance obtained without any training. We study the impact on performance of combining our method with 6 baseline WSOL methods. Our choice is based on low complexity – we chose methods that yield CAMs by a simple forward pass, such as CAM, or a forward and a backward pass, such as GradCAM family while using standard pretrained classifiers. In addition, these methods simply interrogate a classifier without changing its architecture, making the integration of our decoder to the classifier straightforward. To this end, we select the following WSOL methods: CAM, GradCAM, GradCAM++, Smoth-GradCAM, XGradCAM, and LayerCAM. All the baselines use the same pooling method which is a global average pooling [57]. To integrate our F-CAM method, the WSOL baseline method is trained using the classification term in Eq.3 only until convergence. Then, we freeze the classifier, and continue fine-tuning our decoder using the pixel alignment loss in Eq.3. Such separation in training is meant to avoid any undesirable interaction between classification and pixel-wise assignment tasks [3], and to provide clear conclusions about the results. Moreover, it allows the baseline method to converge and yield accurate localization which will be used to guide the decoder’s fine-tuning.

3.2 Comparison with state-of-the-art:

Quantitative comparison. Tab.1 shows the performance obtained with the proposed and baseline methods according to the MaxBoxAcc and PxAP metrics. We observe that results with the 6 selected baselines range from the lower performance using CAM* to the higher performance using LayerCAM. This provides a good scenario to evaluate our method when combined with weak and strong baselines. (Note that compared to the methods reported in [8], GradCAM family reported much higher performance.) Combing our method with each of these baselines yields a considerable improvement for all CAM methods, CNN backbones, and over both datasets. For instance, CAM* alone yields a MaxBoxAcc of 71.5% over CUB using ResNet50. When combined with our method, its performance climbs to 90.3%. The same improvement is observed over OpenImages but with a smaller margin. Note that OpenImages is more challenging than CUB as has a stronger variation among classes of different objects (CUB contains only birds’ species). Results indicate that by

Methods	CUB (MaxBoxAcc)				OpenImages (PxAP)			
	VGG	Inception	ResNet	Mean	VGG	Inception	ResNet	Mean
CAM [57] (cvpr,2016)	71.1	62.1	73.2	68.8	58.1	61.4	58.0	59.1
HaS [34] (iccv,2017)	76.3	57.7	78.1	70.7	56.9	59.5	58.2	57.8
ACoL [53] (cvpr,2018)	72.3	59.6	72.7	68.2	54.7	63.0	57.8	58.4
SPG [54] (eccv,2018)	63.7	62.8	71.4	66.0	55.9	62.4	57.7	58.6
ADL [9] (cvpr,2019)	75.7	63.4	73.5	70.8	58.3	62.1	54.3	58.2
CutMix [51] (eccv,2019)	71.9	65.5	67.8	68.4	58.2	61.7	58.7	59.5
Best WSOL	76.3	65.5	78.1	70.8	58.3	63.0	58.7	59.5
FSL baseline	86.3	94.0	95.8	92.0	61.5	70.3	74.4	68.7
Center baseline	59.7	59.7	59.7	59.7	45.8	45.8	45.8	45.8
CSTN [22] (icpr,2020)	Resnet101 [14]: 76.0				—	—	—	—
TS-CAM [13] (corr,2021)	Deit-S [39]: 83.8				—	—	—	—
MEIL [21] (cvpr,2020)	73.8	—	—	—	—	—	—	—
DANet [47] (iccv,2019)	67.7	67.03	—	—	—	—	—	—
SPOL [44] (cvpr,2021)	—	—	96.4	—	—	—	—	—
CAM* [57] (cvpr,2016)	61.6	58.8	71.5	63.9	53.0	62.7	56.8	57.5
GradCAM [32] (iccv,2017)	69.3	62.3	73.1	68.2	59.6	63.9	60.1	61.2
GradCAM++ [7] (wacv,2018)	84.1	63.3	81.9	76.4	60.5	64.0	60.2	61.5
Smooth-GradCAM++ [25] (corr,2019)	69.7	66.9	76.3	70.9	52.2	61.7	54.3	56.0
XGradCAM [12] (bmvc,2020)	69.3	60.9	72.7	67.6	59.0	63.9	60.2	61.0
LayerCAM [15] (iecc,2021)	84.3	66.5	85.2	78.6	59.5	63.5	61.1	61.3
CAM* [57] + ours	87.3	82.0	90.3	86.5	67.8	71.9	72.1	70.6
GradCAM [32] + ours	87.5	84.4	90.5	87.4	68.6	70.0	70.9	69.8
GradCAM++ [7] + ours	91.5	84.6	91.0	89.0	64.8	67.1	66.3	66.0
Smooth-GradCAM++ [25] + ours	89.1	86.8	90.7	88.8	60.3	65.4	64.4	63.3
XGradCAM [12] + ours	86.8	84.4	90.4	88.8	68.7	71.3	70.4	70.1
LayerCAM [15] + ours	91.0	85.3	92.4	89.7	64.3	64.9	65.3	64.8
Best WSOL + ours	91.5	86.8	92.4	89.7	68.7	71.9	72.1	70.6

Table 1: Performance on MaxBoxAcc and PxAP metrics.

Methods	Top-1 localization			Top-5 localization		
	VGG	Inception	ResNet	VGG	Inception	ResNet
CAM [57] (cvpr,2016)	45.8	40.4	56.1	—	—	—
HaS [34] (iccv,2017)	55.6	41.1	60.7	—	—	—
ACoL [53] (cvpr,2018)	44.8	46.8	57.8	—	—	—
SPG [54] (eccv,2018)	42.9	44.9	51.5	—	—	—
ADL [9] (cvpr,2019)	39.2	35.2	41.1	—	—	—
CutMix [51] (eccv,2019)	47.0	48.3	54.5	—	—	—
ICL [17] (accv,2020)	57.5	56.1	56.1	—	—	—
CSTN [22] (icpr,2020)	Resnet101 [14]: 49.0			—	—	—
TS-CAM [13] (corr,2021)	Deit-S [39]: 71.3			—	—	—
I ² C [55] (eccv,2020)	—	56.0	—	—	68.3	—
MEIL [21] (cvpr,2020)	57.4	—	—	—	—	—
DANet [47] (iccv,2019)	52.5	49.4	—	61.9	60.4	—
NL-CCAM [49] (wacv,2020)	52.4	—	—	65.0	—	—
SPOL [44] (cvpr,2021)	—	—	80.1	—	—	93.4
CAM* [57] (cvpr,2016)	33.5	40.9	47.8	52.7	54.8	66.5
GradCAM [32] (iccv,2017)	18.5	41.6	32.3	41.7	56.2	56.4
GradCAM++ [7] (wacv,2018)	20.8	41.4	34.7	47.5	56.8	61.4
Smooth-GradCAM [25] (corr,2019)	17.7	44.4	33.1	40.2	60.2	57.7
XGradCAM [12] (bmvc,2020)	18.5	40.9	48.3	41.7	55.2	67.3
LayerCAM [15] (iecc,2021)	24.8	43.9	44.2	47.8	59.7	70.3
CAM* [57] + ours	44.0	54.6	59.1	70.1	73.8	82.6
GradCAM [32] + ours	22.1	56.1	38.8	50.0	75.4	68.5
GradCAM++ [7] + ours	23.2	55.9	39.0	52.0	76.0	68.9
Smooth-GradCAM [25] + ours	22.9	57.3	38.9	51.2	77.6	68.6
XGradCAM [12] + ours	22.0	55.8	59.3	49.6	75.3	82.7
LayerCAM [15] + ours	23.1	56.4	47.7	51.9	76.6	76.1

Table 2: Top-1 and Top-5 localization accuracy of WSOL methods on CUB using the MaxBoxAcc metric. In red are the cases where our method decreases performance over the corresponding baseline.

simply combining a decoder with these baselines, we can increase their performance to a level that is competitive with recent state-of-the-art methods, such as TS-CAM and CSTN and even approaching the performance of SPOL. In addition,

these results are competitive with FSL, and in some cases, surpassing FSL performance. Similar behavior is observed over MaxBoxAccV2 performance⁴.

Tab.2 show top-1/5 localization performance over CUB. When using our method, WSOL baselines obtained competitive top-5 localization over Inception and ResNet architectures. However, top-1 localization is poor even with the assistance of our method. Because top-1 localization is directly tied to classification performance, the improvement of our method is bounded by the number of correctly classified samples. By inspecting the classification performance of WSOL baselines, only CAM* yields high accuracy over the CUB dataset for the three architectures. This explains why top-1 CAM* is much higher than others. The average classification accuracy ranges from 44% to 59%. In addition, all WSOL baselines yield high classification using VGG16 over CUB which again explains the high top-1 localization. Over OpenImages, all methods yield relatively the same classification accuracy with an average that ranges from 63% to 70%. Full report of classification performance is presented in supplementary material. Since we aim in our method only to improve localization performance without changing the classification performance, our method can only improve the localization of correctly classified samples. This gives advantage to other methods that have high classification accuracy. Note that model selection during the training of our baselines is achieved through the localization performance on the validation set as proposed in [8]. It was observed in [8] that the localization task converges in the early training epochs while the classification task takes longer to converge. We observed similar behavior when training our baselines⁵.

Visual comparison: WSOL baselines with F-CAMs. Fig. 3, 4 illustrate the impact of our method on WSOL baselines in term of activations and localization. It is well known that standard CAM methods tend to activate only over minimal discriminative regions as shown in these figures. However, the optimum threshold allows other tiny (invisible) activations to participate in defining the final localization such as in the first row in Fig. 3. As a result, non-discriminative regions could be easily included in the localization. Moreover, it downgrades the interpretability aspect since the box contains regions without any visible activation. In comparison, our method yields sharp and complete CAMs allowing bounding boxes to be tight around the object making it robust to thresholding while improving the interpretability aspect. Similarly, over Open-Images, WSOL baselines yield minimal activation that are sensitive to thresholding. Note that in $P \times AP$ metric, authors in [8] do not define an optimum threshold as in $MaxBoxAcc$.

⁴MaxBoxAccV2 performance over CUB is reported in supplementary material

⁵Training curves and the classification performance of all WSOL baselines methods are reported in the supplementary material.

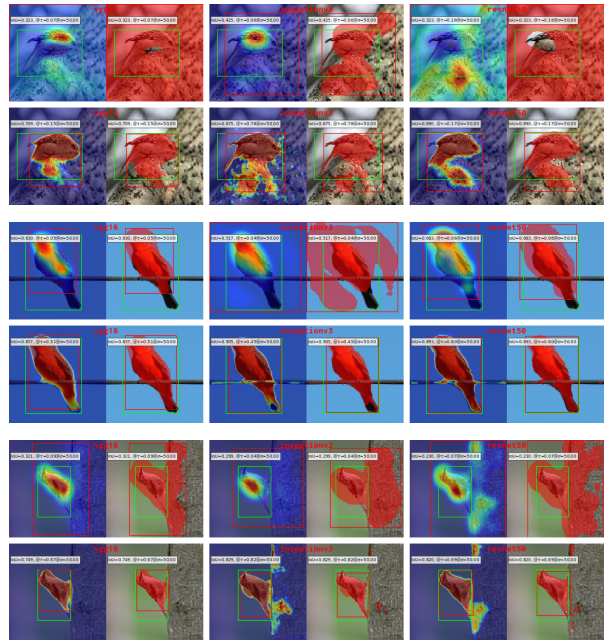


Figure 3: Test samples from CUB. Top: CAM*. Middle: GradCAM. Bottom: GradCAM++. First row: WSOL baseline. Next row: WSOL baseline + ours. First column: CAM. Next column: localization. Colors: boxes: predicted in red and true box is in green. Thresholded mask is in red. $\sigma = 50\%$.

and `MaxBoxAccV2` since `PxAP` defines an area under the precision-recall curve. Using high threshold such as .8 yields very small true positive regions with high false negative. In the other hand, our method easily covers the object with minimal false positive. We present next an analysis to the score in the CAMs as an attempt to understand the sensitivity of CAMs to thresholding.

Activation distribution shift: WSOL baselines with F-CAMs. Fig.5 shows the change in MaxBoxAcc and PxAP metrics with respect to τ over the test set using CAM* baseline compared to CAM* + ours⁶. For MaxBoxAcc metric, notice that the CAM*'s functioning region is concentrated near 0 while the performance completely drops to zero when τ starts to increase. This indicates that often the optimum threshold for these method is very small. In the other hand, when combined with our method, MaxBoxAcc becomes less sensitive to τ . Over PxAP metric (Fig.5b), using our method improve the metric by pushing the curve to the top right corner. Following [8], we inspect the CAM's activation distribution since they are related to defining the shape of the metrics curves (Fig.6). CAM* shows a single mode with high concentration of activation near zero which explains the shape of the MaxBoxAcc and PxAP metrics (Fig.5). In addition,

⁶The rest of the methods are presented in the supplementary material.

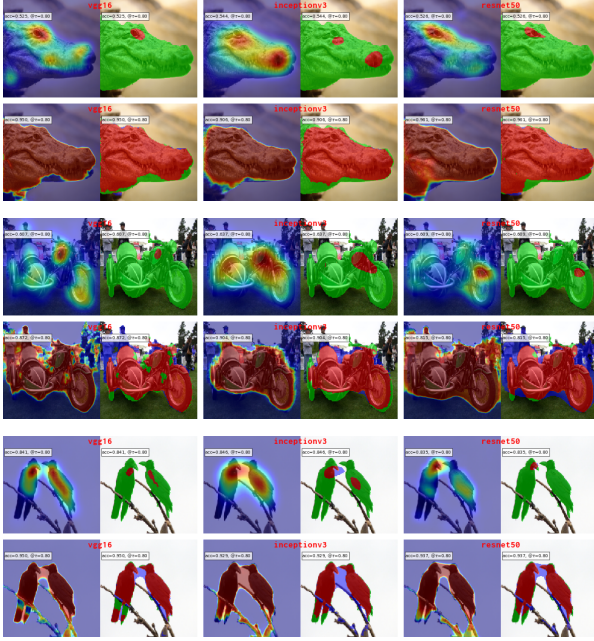
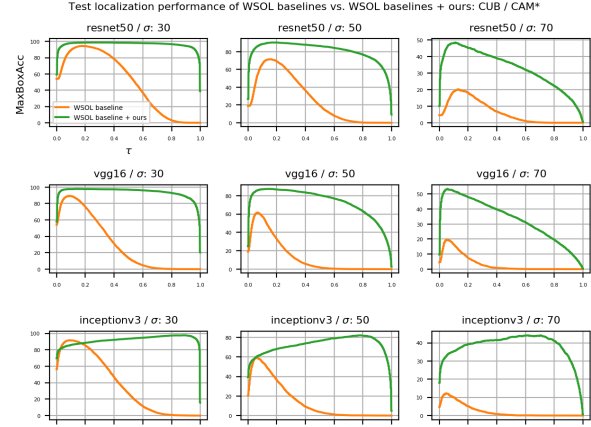
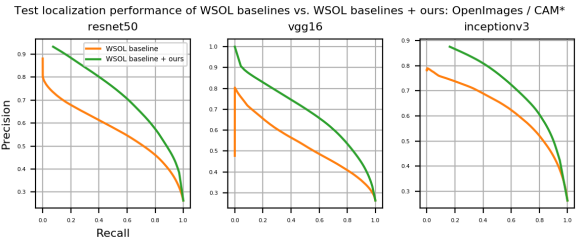


Figure 4: Test samples from OpenImages. Top: LayerCAM. Middle: Smooth-GradCAM. Bottom: XGradCAM. First row: WSOL baseline. Next row: WSOL baseline + ours. First column: CAM. Next column: localization. Colors: green false negative, red : true positive, blue: false positive. $\tau = .8$.

tion, this makes the search of the optimum threshold difficult. Moreover, changing slightly the threshold could lead to high variation in localization performance since the threshold is expected to separate foreground from background. The high concentration of activation means that the method is unable to separate both regions and reflects more uncertainty downgrading furthermore CAM’s interpretability. In the other hand, using our method allows the appearance of a second mode near one. This second mode is more clear over OpenImages dataset. Moreover, both modes are sharper than CAM* alone. This reflects more certainty of assigning foreground and background to each pixel. The reason for this behavior is that our activations are trained using cross-entropy (Eq.3) which pushes activations to be certain (0/1). These results explain why metrics over baseline CAM* perform well only near zero with large sensitivity to thresholding while our method shows less sensitivity. It is important to note that CAM’s activation distribution (Fig.6) is heavily influenced with the object size. For datasets with small objects, background pixels which are expected to have low activation will lead typically to density around zero that is higher than the density around one. This can be observed over CUB for our method. In the other hand, over datasets with large objects, density around one are typically expected to be high which is observed over OpenImages using our method.



(a) MaxBoxAcc metric.



(b) P_{xAP} metric.

Figure 5: Metrics variations vs. threshold τ : CAM* (orange) vs. CAM* + ours (green).

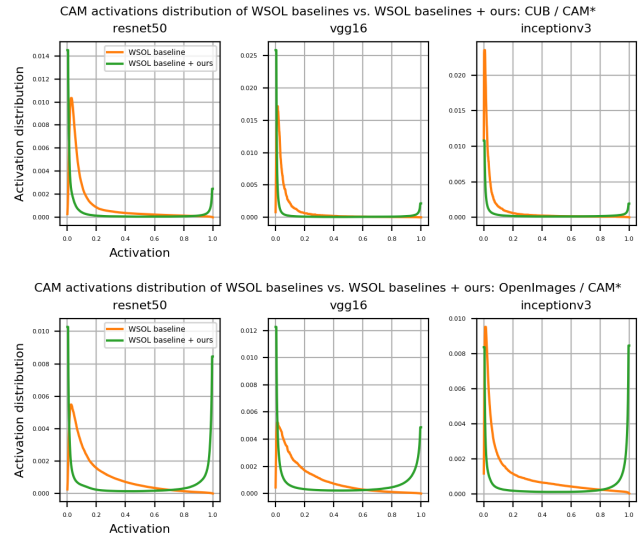


Figure 6: Activation distributions over entire test set: CAM* (orange) vs. CAM* + ours (green). Top: CUB. Bottom: OpenImages.

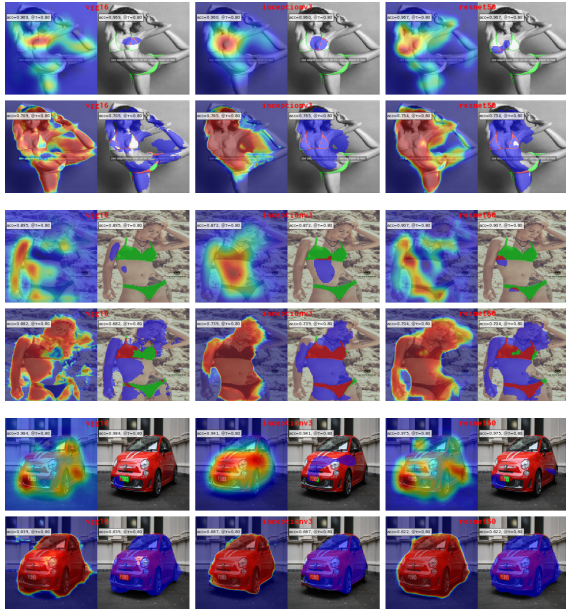


Figure 7: Failed cases of our method combined with CAM* over OpenImages test set. Colors: green: false negative, red: true positive, blue: false positive. $\tau = .8$.

Complexity. We report inference runtime of WSOL baselines and our method in the supplementary material.

Failure cases. Fig. 7 illustrates few examples over OpenImages test set where our method failed to localize the correct object. The fine-tuning of our method is guided mainly by the activations of the WSOL baseline. When the activations largely miss the correct object, our method learns on wrong supervisory signal leading to false localization. Detecting these cases and dealing with them remains an open issue in this work. This scenario goes under learning from highly noisy supervisory signals which is still a growing field [35].

3.3 Ablation study

Tab. 3 shows the impact of adding different terms in the pixel alignment loss in Eq. 3 on all backbones and both datasets using CAM* method. We observe that simply adding sampling regions of foreground and background yields a large improvement of the baseline. This shows the importance of using supervisory signals at pixel level to guide CAMs. Baseline methods use only classification signal which is a global information. Adding local guidance helps better discerning foreground from background. Adding a CRF term and size constraint helps better extending the foreground while respecting object’s boundaries yielding more improvement. We report in Fig. 8 the impact of the hyper-parameter n^- on the localization performance. n^- describes the extent of the background region we are allowed to sample from. It is in-

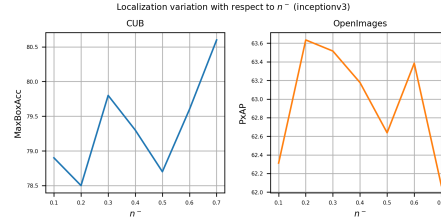


Figure 8: Impact of n^- on the localization performance over CUB and OpenImages validation with CAM* baseline + ours. Random runs are done while the rest of hyper-parameters are fixed.

terconnected with the object size. Datasets with large object result in small background and small objects lead to large background. This is reflected in these curves. On CUB, often objects are small. Therefore, assuming large background is safe. As a result, large values of n^- yield better results. On the other hand, objects in OpenImages dataset tend to be large leaving small background making small values of n^- more efficient.

Methods	CUB (MaxBoxAcc)				OpenImages (PAP)			
	VGG	Inception	ResNet	Mean	VGG	Inception	ResNet	Mean
CAM* [57]	61.6	58.8	71.5	63.9	53.0	62.7	56.8	57.5
CAM* [57] + SR	84.2	73.0	82.2	79.8	64.5	64.1	63.8	64.1
CAM* [57] + SR + CRF	84.6	78.9	86.1	83.2	66.3	68.3	67.5	67.3
CAM* [57] + SR + CRF + ASC	87.3	82.0	90.3	86.5	67.8	71.9	72.1	70.6
Improvement	+25.7	+23.2	+18.8	+22.5	+14.8	+9.2	+15.3	+12.8

Table 3: Ablation study of different terms in the pixel alignment loss (Eq. 3) over CAM* baseline. The bottom line in green is the improvement over the WSOL baseline CAM* (top green line), when combined with our full method 4th green line.

Note. Supplementary material contains: code, more visual results, convergence curves of WSOL baselines, and more CAMs analysis.

4 Conclusion

CAM methods typically rely on interpolation in order to restore full size CAMs in WSOL tasks. To improve the localization accuracy of CAMs, this paper proposes to connect a trainable decoding architecture to any CNN backbone, allowing for parametric upscaling of CAMs to accurate full resolution CAMs (F-CAMs). Low resolution CAMs and variants priors are used to fine-tune the decoder. Evaluated in combination with six baseline WSOL methods and three CNN backbones, our F-CAM methods improves their performance by a large margin on CUB and OpenImage datasets. F-CAM performance is competitive with state-of-art WSOL methods, yet it requires fewer computational resources during inference.

Acknowledgment

This research was supported in part by the Canadian Institutes of Health Research, the Natural Sciences and Engineering Research Council of Canada, Compute Canada, MITACS, and the Ericsson Global AI Accelerator Montreal.

A Supplementary material

You find in this supplementary material:

1. Runtime inference for WSOL baselines and our method (Tab.A.2).
2. MaxBoxAccV2 performance over CUB (Tab.A.1).
3. Classification performance of different WSOL baselines (Tab.A.3).
4. Convergence curves of WSOL baseline training. (Fig.A.5).
5. Comparison of localization performance curves (Fig.A.3,A.4).
6. Comparison to CAMs activations distributions (Fig.A.1, A.2)

Complexity. We report in Tab.A.2 the time required to build a CAM for all the studied WSOL baselines and other methods. While adding a decoder to a standard classifier increases the number of parameters, the inference time is still better than average baselines. Because the inference is achieved through a single forward with fully convolutional operations, our method is expected to be fast. Other methods may require a forward and a backward to estimate a CAM. Our method is still competitive to ACoL, SPG, and ADL methods. We included other methods ScoreCAM [43], SSCAM [54], and IS-CAM [23]. Their slow runtime prevented us from considering them as baselines.

Methods	CUB (MaxBoxAccV2)			
	VGG	Inception	ResNet	Mean
CAM [57](cvpr,2016)	63.7	56.7	63.0	61.1
HaS [34](iccv,2017)	63.7	53.4	64.7	60.6
ACoL [53] (cvpr,2018)	57.4	56.2	66.5	60.0
SPG [54](eccv,2018)	56.3	55.9	60.4	57.5
ADL [9] (cvpr,2019)	66.3	58.8	58.4	61.1
CutMix [51](eccv,2019)	62.3	57.5	62.8	60.8
Best WSOL	66.3	58.8	66.5	61.1
FSL baseline	71.6	86.6	82.4	80.2
Center baseline	59.7	59.7	59.7	59.7
ICL [17](accv,2020)	66.7	60.3	63.2	63.4
CAM* [57] (cvpr,2016)	57.0	54.4	62.1	57.8
GradCAM [32] (iccv,2017)	62.7	57.1	63.3	61.0
GradCAM++ [7] (wacv,2018)	73.8	60.7	70.2	68.2
Smooth-GradCAM++ [25] (corr,2019)	64.1	59.7	66.6	63.4
XGradCAM [12] (bmvc,2020)	62.8	56.7	63.2	60.9
LayerCAM [15] (ieee,2021)	74.1	62.6	72.6	69.7
CAM* [57] + ours	79.1	71.2	79.4	76.5
GradCAM [32] + ours	79.5	76.2	80.8	78.5
GradCAM++ [7] + ours	84.1	73.1	82.7	79.9
Smooth-GradCAM++ [25] + ours	83.1	74.0	81.6	79.5
XGradCAM [12] + ours	80.1	70.6	80.0	76.9
LayerCAM [15] + ours	84.3	73.9	82.7	80.3
Best WSOL + ours	84.3	76.2	82.7	80.3

Table A.1: Performance on CUB using MaxBoxAccV2 metric.

Backbones (encoders) Methods	VGG16				Inception				ResNet50			
	#PCL	#NFM	SFM	#PDEC	#PCL	#NFM	SFM	#PDEC	#PCL	#NFM	SFM	#PDEC
Details	≈ 19.6	1024	28x28	≈ 23.1	≈ 25.6	1024	28x28	≈ 5.7	≈ 23.9	2048	28x28	≈ 9
CAM* [57]			.2ms				.2ms				.3ms	
GradCAM [32]			7.7ms				21.1ms				27.8ms	
GradCAM++ [7]			23.5ms				23.7ms				28.0ms	
Smooth-GradCAM [25]			62.0ms				150.7ms				136.2ms	
XGradCAM [12]			2.9ms				19.2ms				14.2ms	
LayerCAM [15]			3.2ms				18.2ms				17.9ms	
Mean			16.6ms				38.8ms				37.4ms	
ours + STDCL			6.2ms				25.5ms				18.5ms	
ACoL [53]			12.0ms				19.2ms				24.9ms	
SPG [54]			11.0ms				18ms				23.9ms	
ADL [9]			6.4ms				16.0				14.4ms	
ScoreCAM [43]			1.9sec				3.4sec				9.3sec	
SSCAM [24]			1min45sec				2min16sec				5min49sec	
IS-CAM [23]			30.1sec				39.0sec				1min39sec	

Table A.2: Time required to build CAMs of different WSOL methods. **STDCL**: standard classifier = encoder (VGG16, Inception, ResNet50) + global average pooling. **#PCL** (millions): number of the parameters of the classifier. **#NFM**: number of the feature maps at the top layer. **SFM**: size of the feature maps at the top layer. **#PDEC** (millions): number of the parameters of the decoder. **Time**: time necessary top build a full size CAM over an idle Tesla P100 GPU for one random RGB image of size 224×224 with 200 classes. Methods SSCAM [24] ($N = 35, \sigma = 2$), IS-CAM [23] ($N = 10$), IS-CAM [23] ($N = 10$) are evaluated with batch size 32 with their original hyper-parameters (N , and σ).

Methods	CUB				OpenImages			
	VGG	Inception	ResNet	Mean	VGG	Inception	ResNet	Mean
CAM [57]	26.8	61.8	58.4	49.0	67.3	36.6	72.6	58.8
HaS [34]	70.9	69.9	74.5	71.8	60.0	68.4	74.0	67.5
ACoL [53]	56.1	71.6	64.0	63.9	68.2	40.7	70.7	59.9
SPG [54]	63.1	58.8	37.8	53.2	71.7	43.5	65.4	60.2
ADL [9]	31.1	45.5	32.7	36.4	66.1	46.6	56.1	56.3
CutMix [51]	29.2	70.2	55.9	51.8	68.1	53.1	73.7	65.0
CAM* [57]	49.3	65.5	65.1	59.9	69.1	61.2	73.2	67.8
GradCAM	24.8	65.4	42.2	44.1	69.0	54.0	72.4	65.1
GradCAM++	24.8	65.2	42.2	44.0	70.3	69.6	72.3	70.7
Smooth-GradCAM	24.8	65.3	42.2	44.1	69.0	54.0	67.0	63.3
XGradCAM	24.8	65.4	65.1	51.7	69.0	69.4	72.0	70.1
LayerCAM	24.8	65.0	51.2	47.0	70.3	53.9	72.2	65.4

Table A.3: Classification performance of WSOL baseline methods. Model selection is performed over localization performance MaxBoxAcc and PxAP.

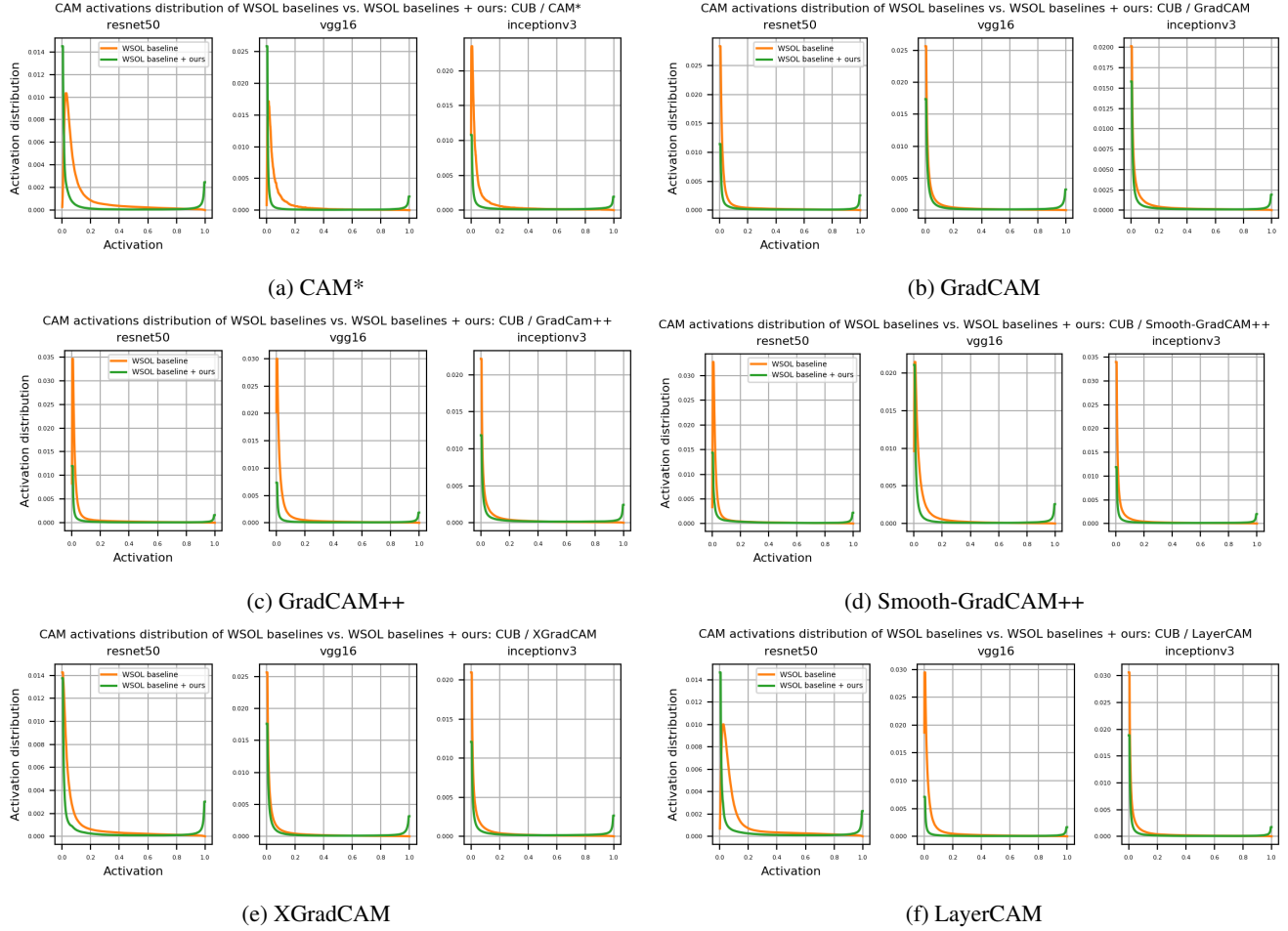
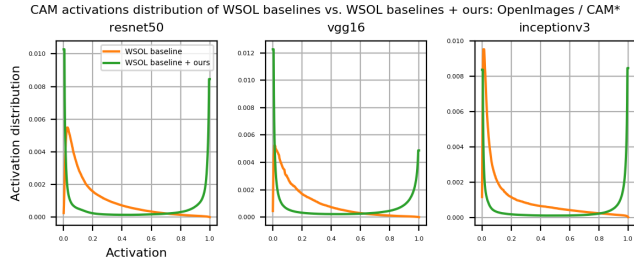
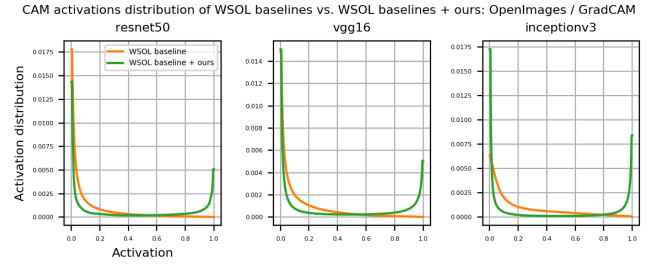


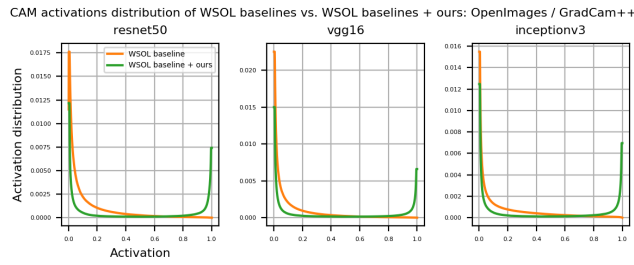
Figure A.1: CAM's activation distribution over CUB test set: WSOL baselines vs. WSOL baseline + ours validated with MaxBoxAcc.



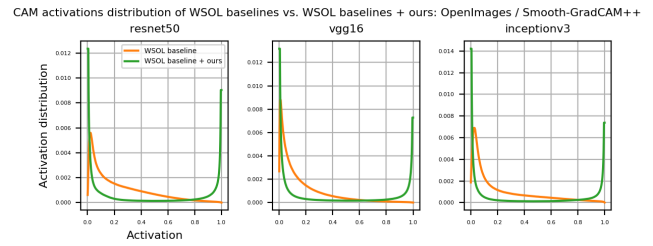
(a) CAM*



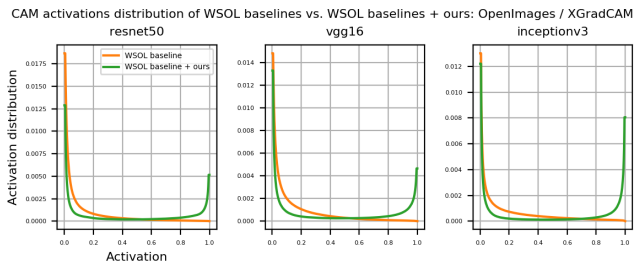
(b) GradCAM



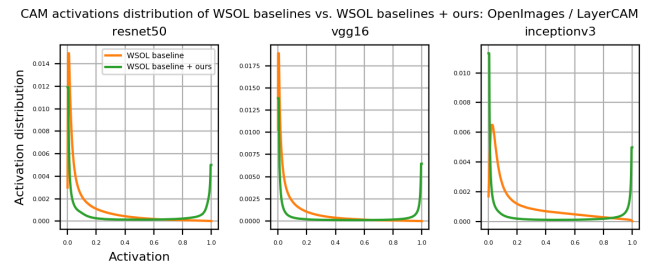
(c) GradCAM++



(d) Smooth-GradCAM++



(e) XGradCAM



(f) LayerCAM

Figure A.2: CAM's activation distribution over OpenImages test set: WSOL baselines vs. WSOL baseline + ours validated with MaxBoxAcc.

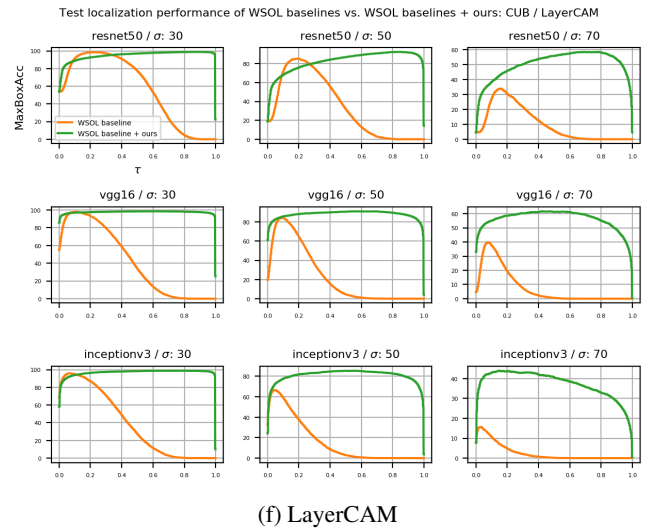
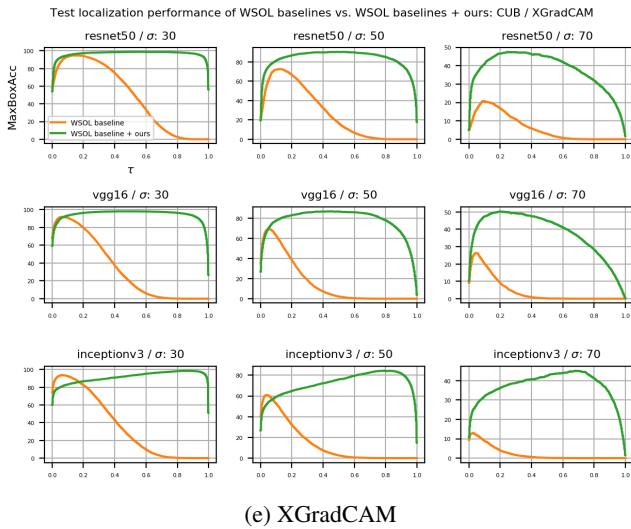
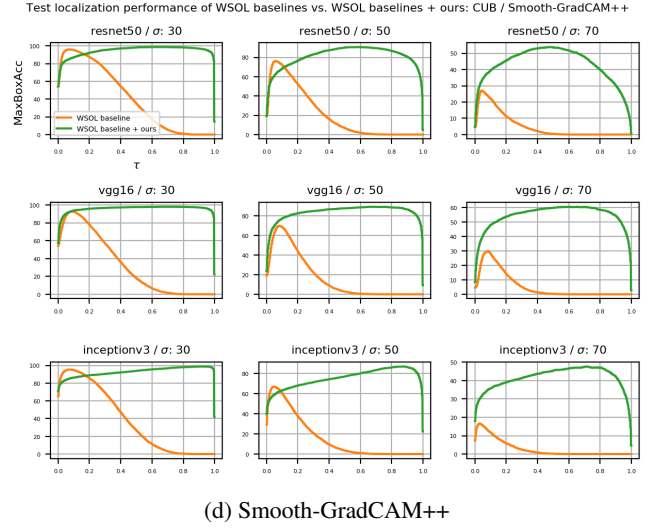
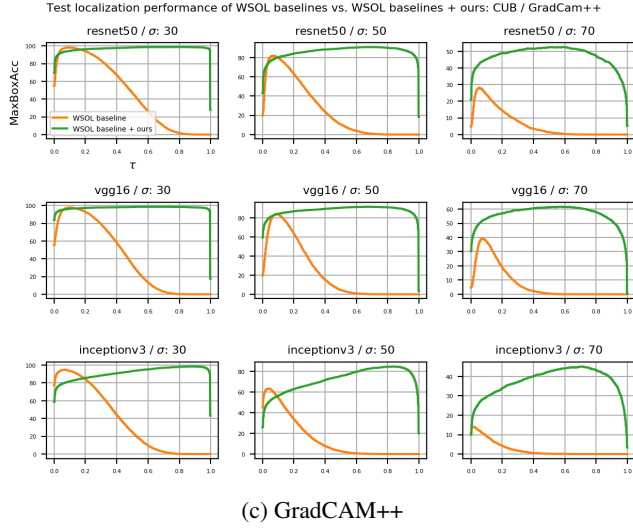
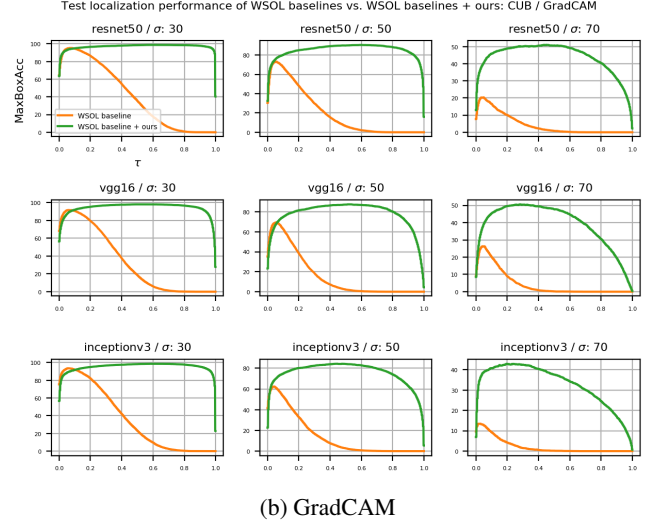
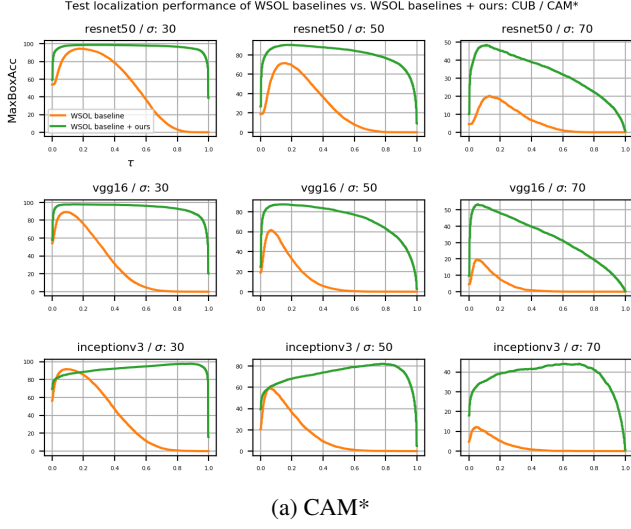
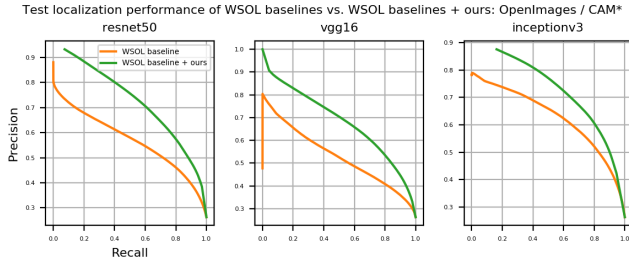
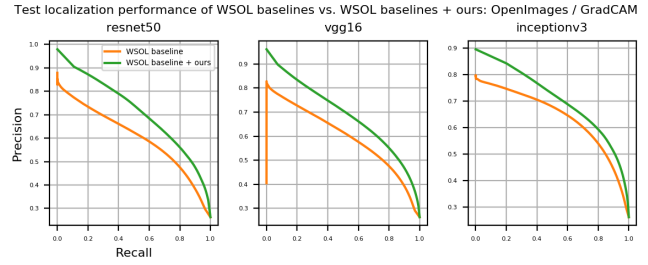


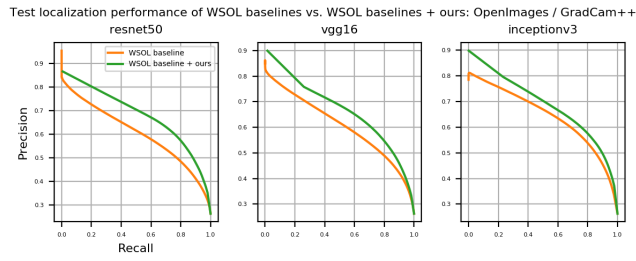
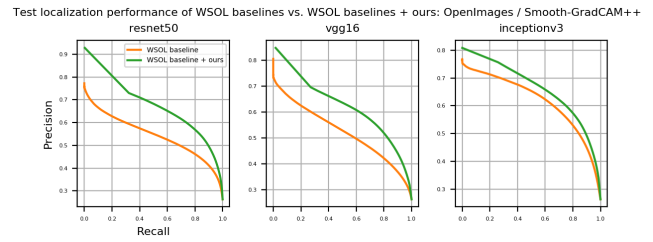
Figure A.3: CUB test set: WSOL baselines vs. WSOL baselines + ours validated with MaxBoxAcc.



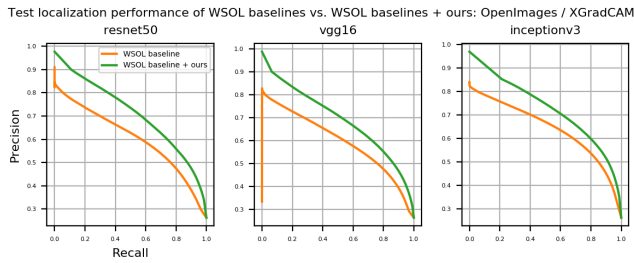
(a) CAM*



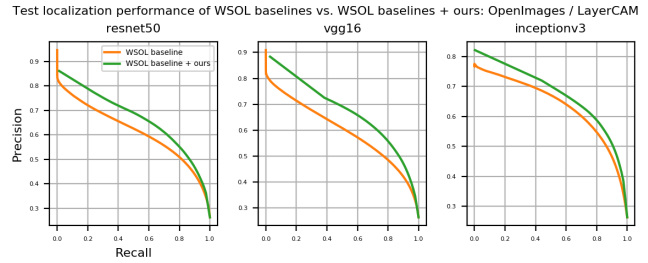
(b) GradCAM

(c) GradCAM++
Aydin Sarraf

(d) Smooth-GradCAM++



(e) XGradCAM



(f) LayerCAM

Figure A.4: OpenImages test set: WSOL baselines vs. WSOL baselines + ours validated with MaxBoxAcc.

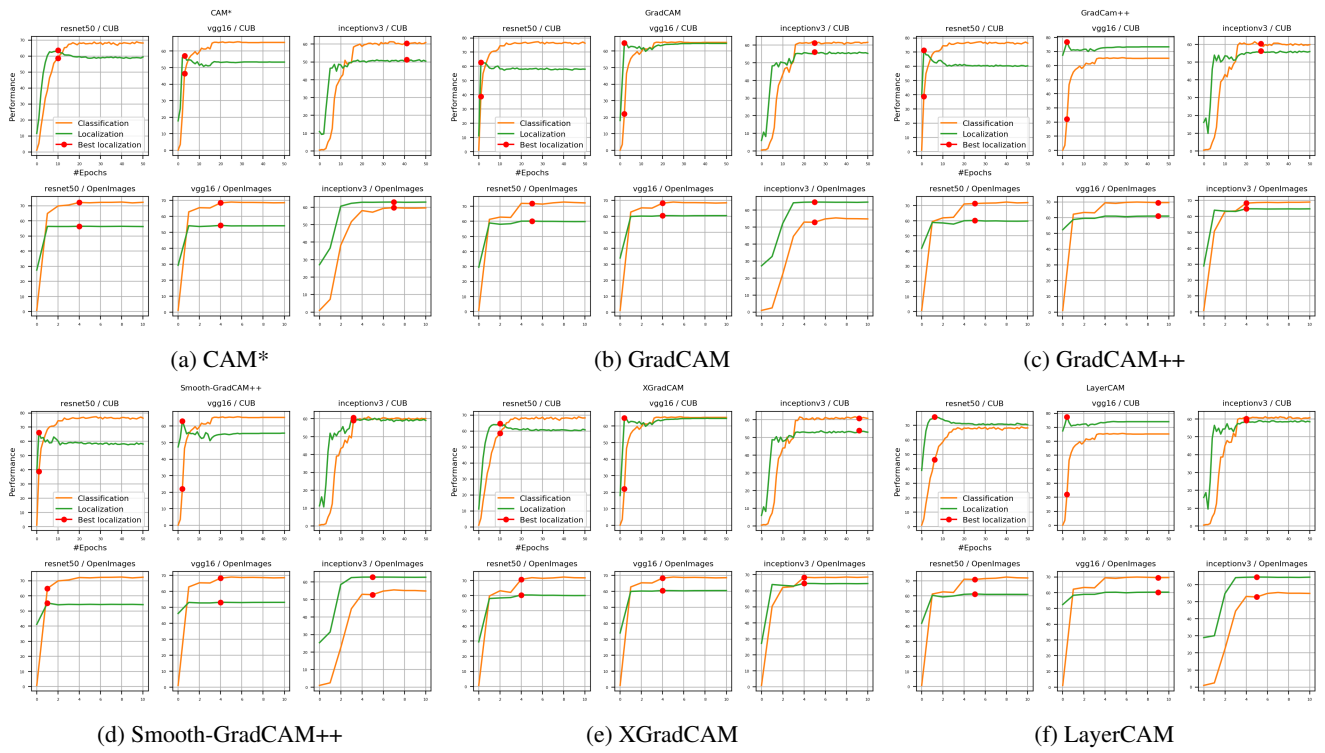


Figure A.5: Convergence of classification and localization tasks over validation set over baselines WSOL methods. The red dot is the epoch for the selected model based on the localization performance using MaxBoxAcc metric.

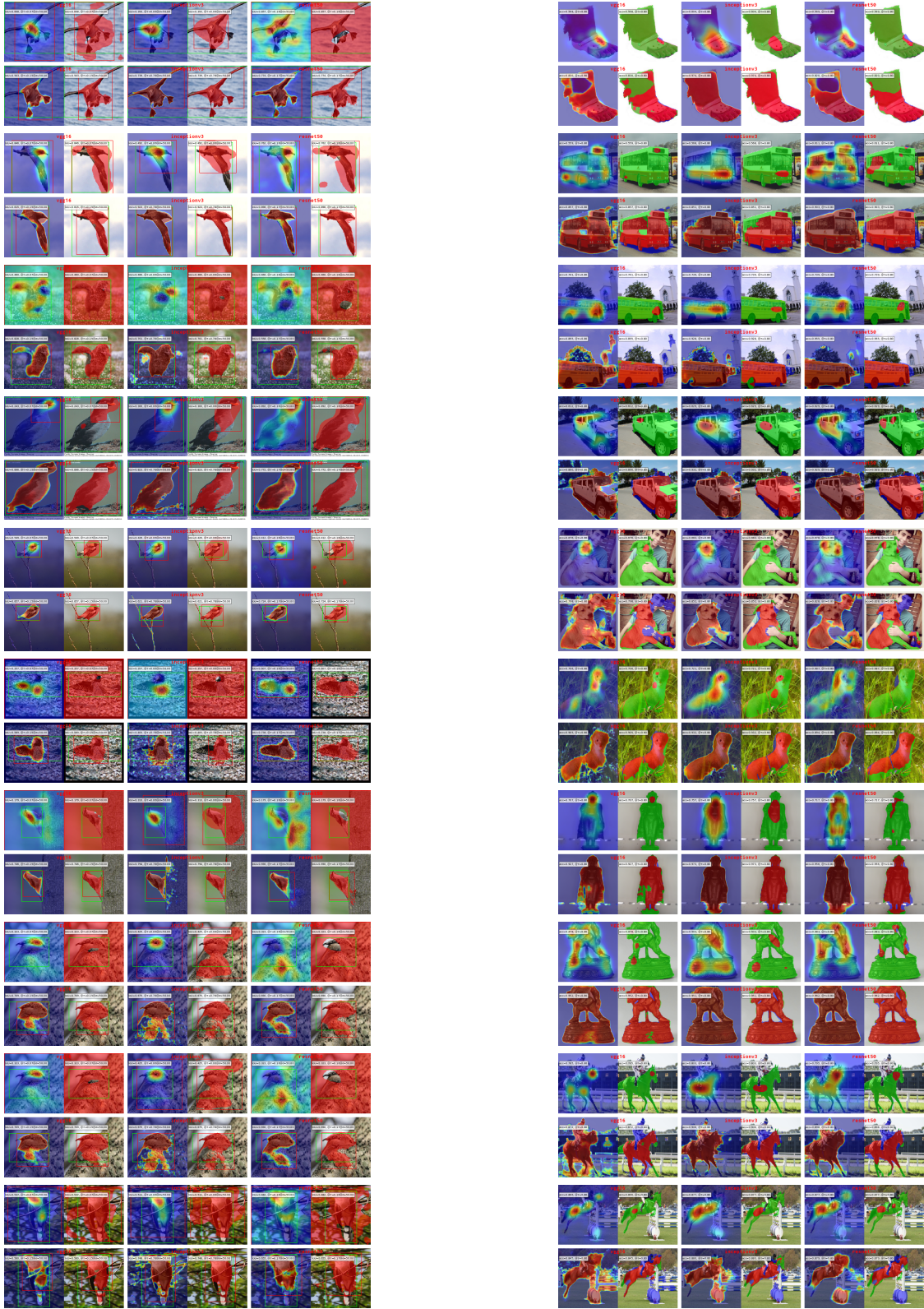


Figure A.6: CAM* method examples for three backbones (left to right: VGG16, Inceptionv3, ResNet50): baselines (top) vs. baseline + ours (bottom) validated with MaxBoxAcc . Colors: CUB (left): green box : ground truth. red box : predicted. red mask: thresholded CAM. OpenImages (right): red mask: true positive. green mask: false negative. blue mask: false positive. $\tau = 50, \sigma = 0.8$.

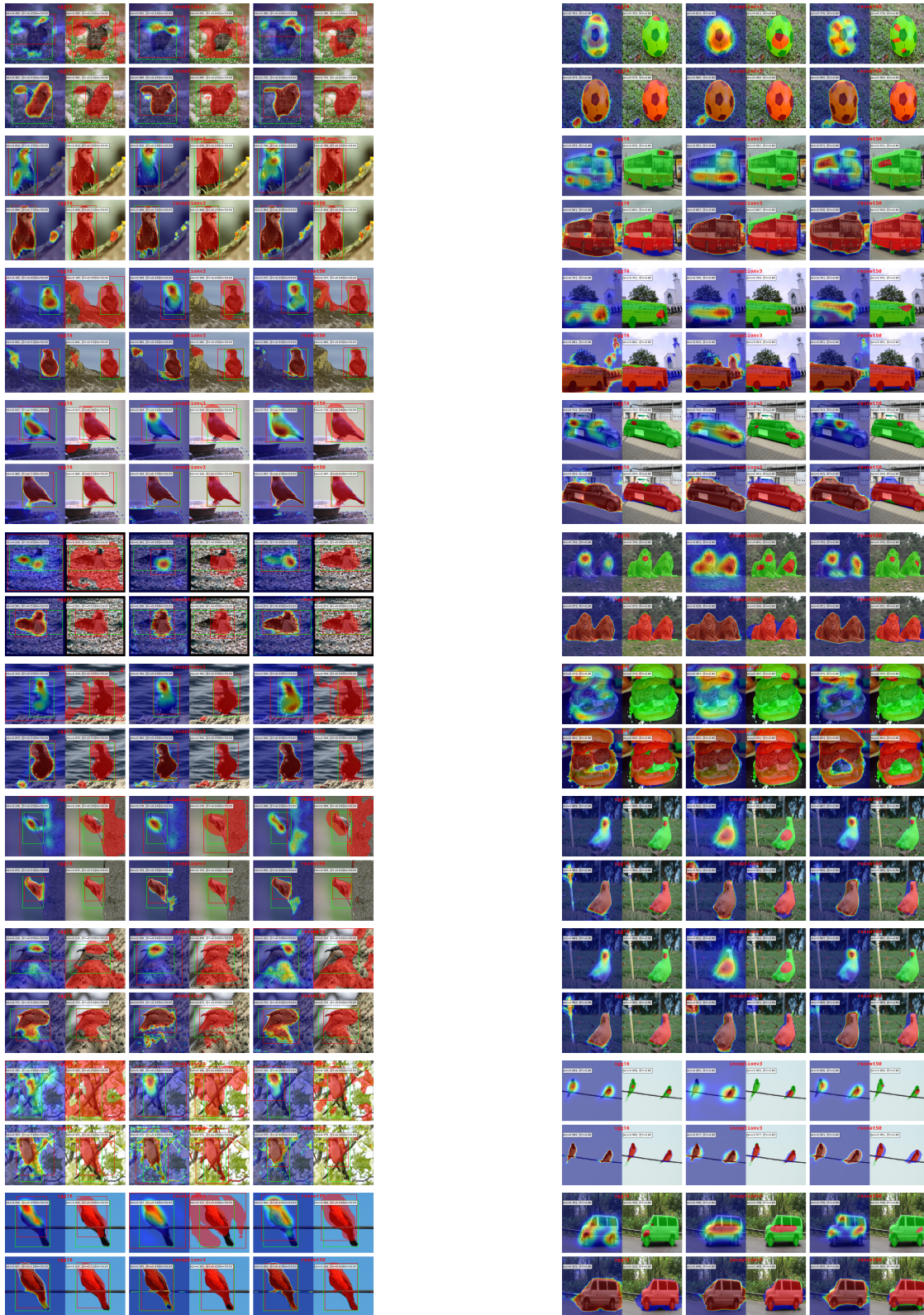


Figure A.7: GradCAM method examples for three backbones (left to right: VGG16, Inceptionv3, ResNet50): baselines (top) vs. baseline + ours (bottom) validated with MaxBoxAcc . Colors: CUB (left): green box : ground truth. red box: predicted. red mask: thresholded CAM. OpenImages (right): red mask: true positive. green mask: false negative. blue mask: false positive. $\tau = 50, \sigma = 0.8$.

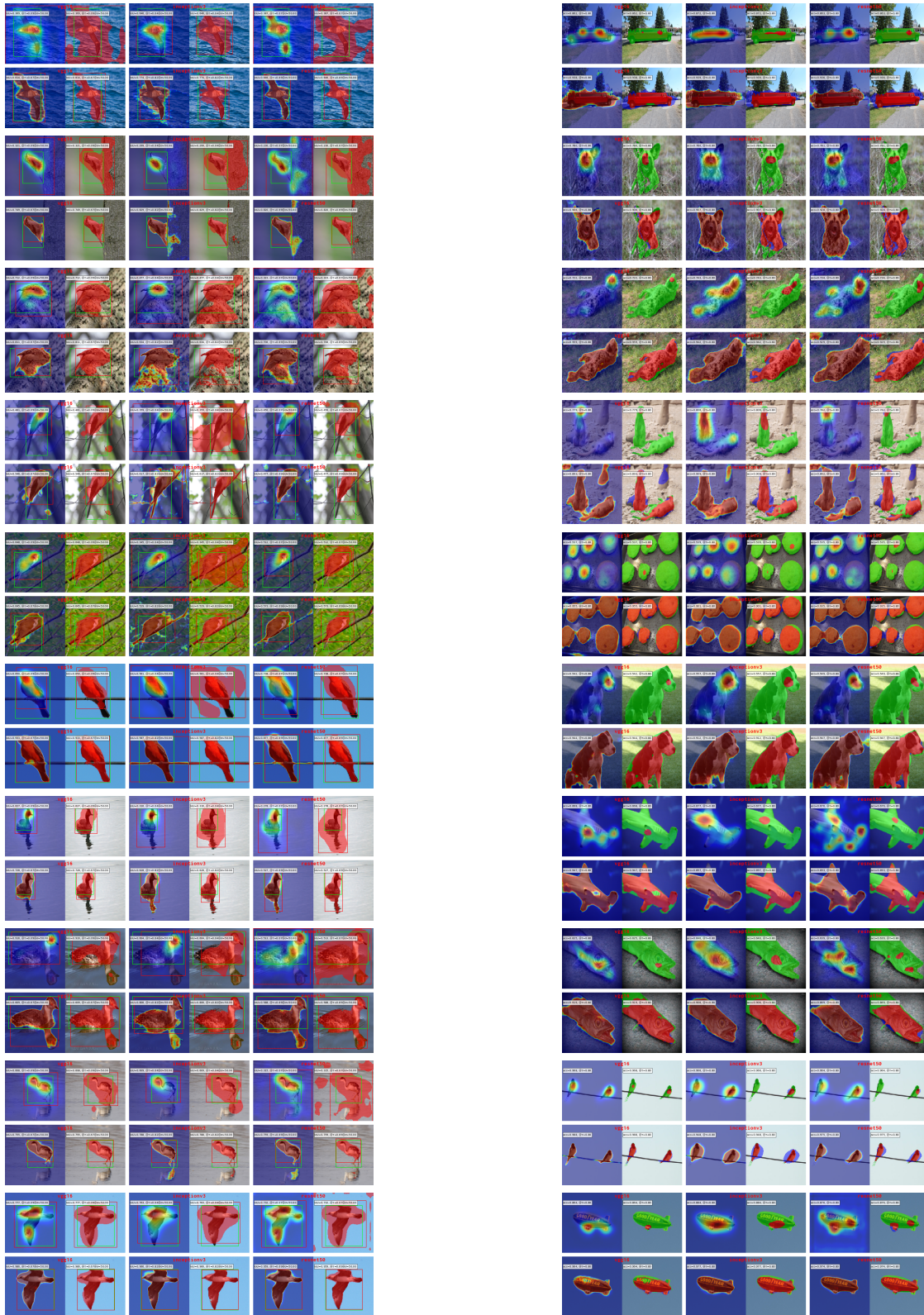


Figure A.8: GradCAM++ method examples for three backbones (left to right: VGG16, Inceptionv3, ResNet50): baselines (top) vs. baseline + ours (bottom) validated with MaxBoxAcc . Colors: CUB (left): green box : ground truth. red box: predicted. red mask: thresholded CAM. OpenImages (right): red mask: true positive. green mask: false negative. blue mask: false positive. $\tau = 50, \sigma = 0.8$.

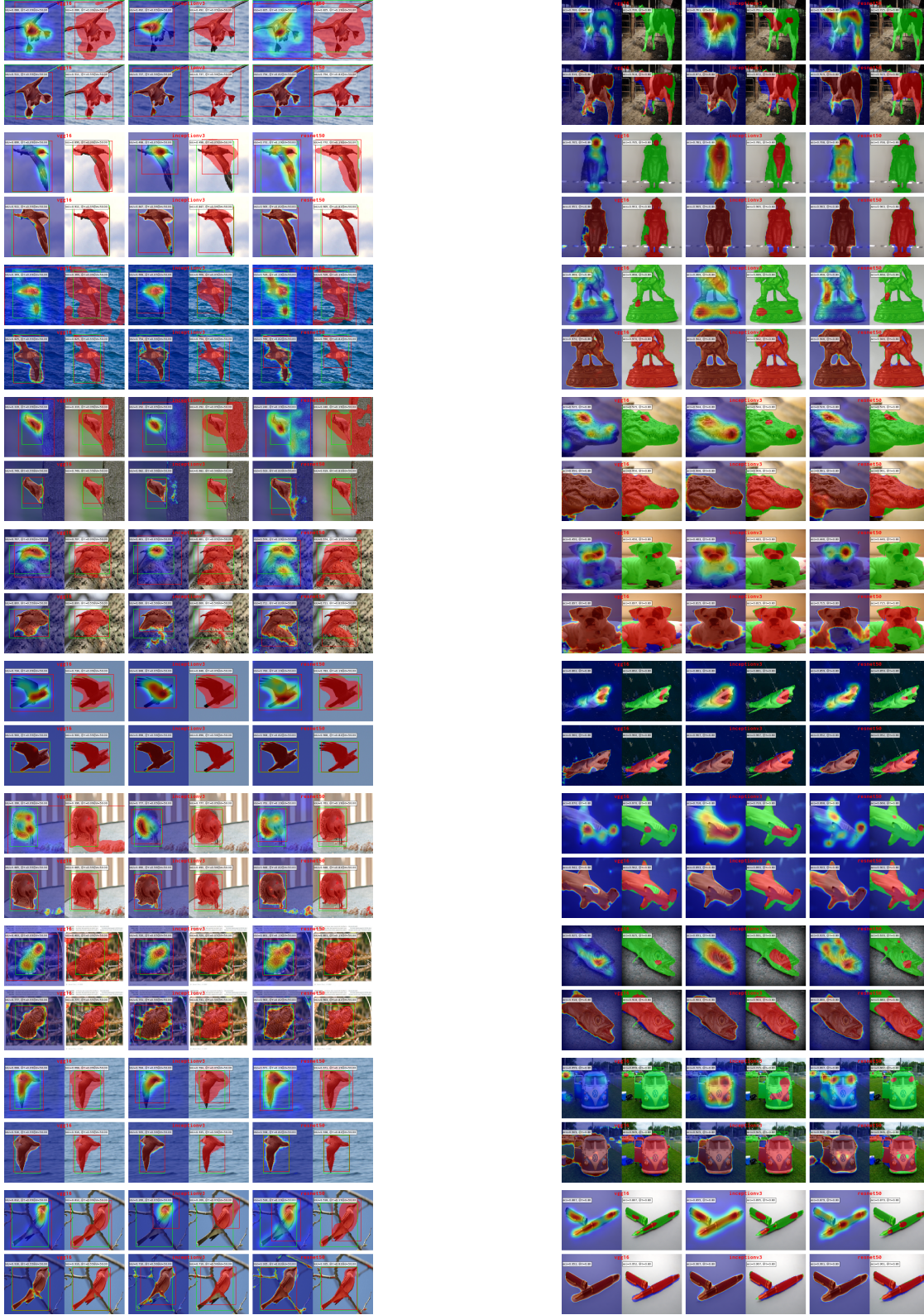


Figure A.9: LayerCAM method examples for three backbones (left to right: VGG16, Inceptionv3, ResNet50): baselines (top) vs. baseline + ours (bottom) validated with MaxBoxAcc . Colors: CUB (left): green box : ground truth. red box: predicted. red mask: thresholded CAM. OpenImages (right): red mask: true positive. green mask: false negative. blue mask: false positive. $\tau = 50, \sigma = 0.8$.

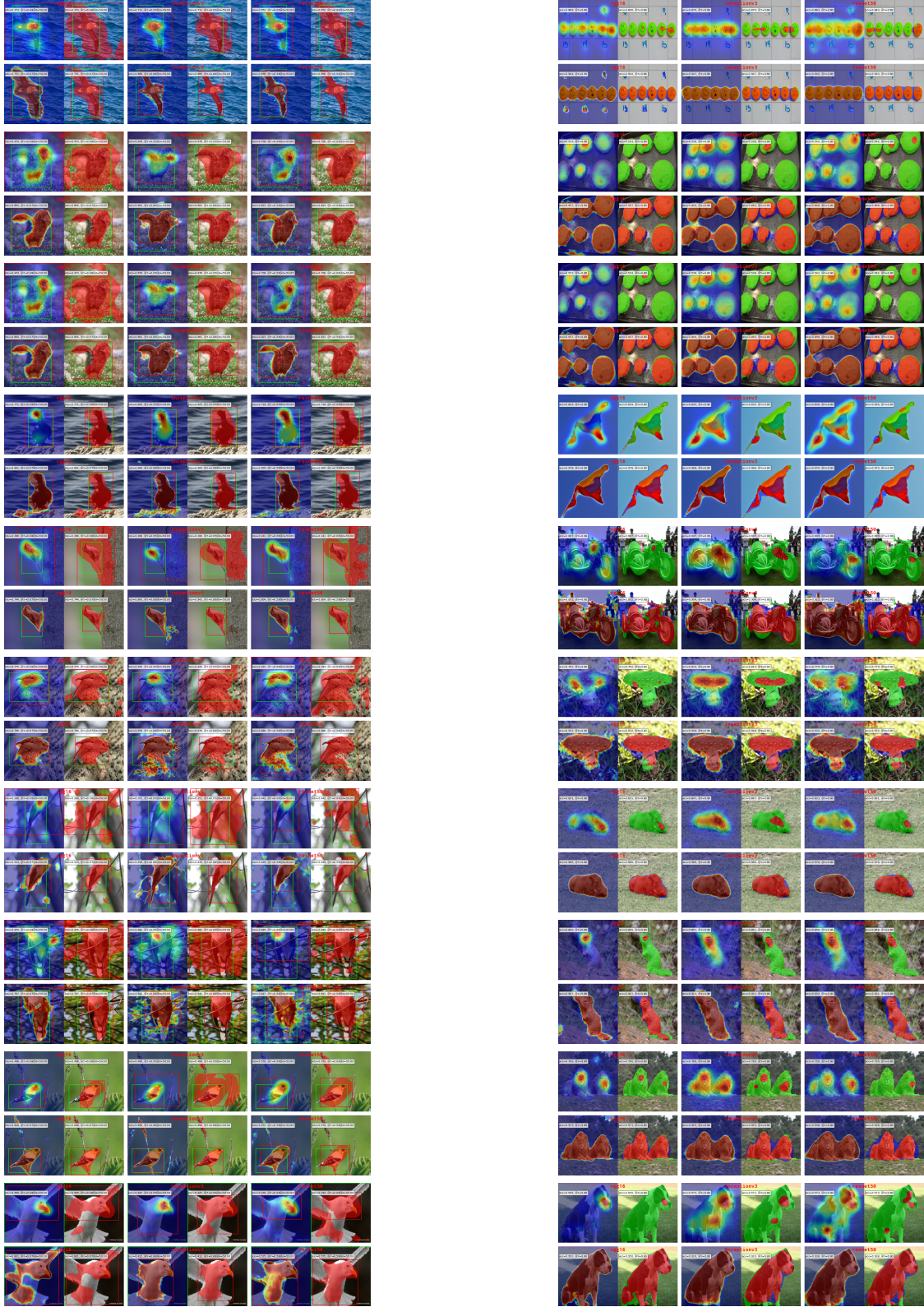


Figure A.10: SmoothGradCAM++ method examples for three backbones (left to right: VGG16, Inceptionv3, ResNet50): baselines (top) vs. baseline + ours (bottom) validated with `MaxBoxAcc`. Colors: CUB (left): green box : ground truth. red box: predicted. red mask: thresholded CAM. OpenImages (right): red mask: true positive. green mask: false negative. blue mask: false positive. $\tau = 50, \sigma = 0.8$.

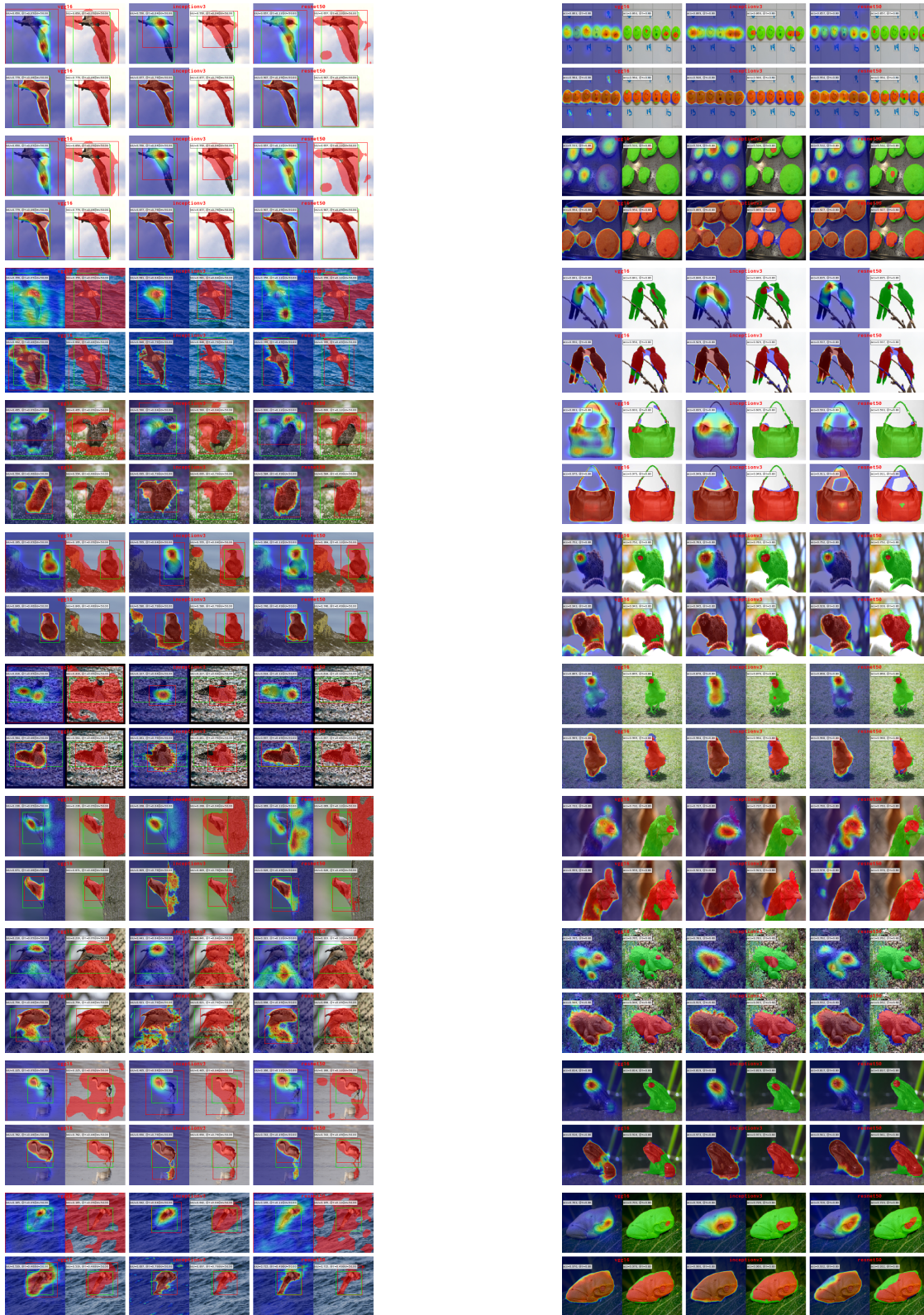


Figure A.11: XGradCAM method examples for three backbones (left to right: VGG16, Inceptionv3, ResNet50): baselines (top) vs. baseline + ours (bottom) validated with MaxBoxAcc . Colors: CUB (left): green box : ground truth. red box: predicted. red mask: thresholded CAM. OpenImages (right): red mask: true positive. green mask: false negative. blue mask: false positive. $\tau = 50, \sigma = 0.8$.

References

- [1] W. Bae, J. Noh, and G. Kim. Rethinking class activation mapping for weakly supervised object localization. In *ECCV*, 2020.
- [2] S. Belharbi, I. Ben Ayed, L. McCaffrey, and E. Granger. Deep ordinal classification with inequality constraints. *CoRR*, abs/1911.10720, 2019.
- [3] S. Belharbi, I. Ben Ayed, L. McCaffrey, and E. Granger. Deep active learning for joint classification & segmentation with weak annotator. In *WACV*, 2021.
- [4] S. Belharbi, J. Rony, J. Dolz, I. Ben Ayed, L. McCaffrey, and E. Granger. Deep interpretable classification and weakly-supervised segmentation of histology images via max-min uncertainty. *CoRR*, abs/2011.07221, 2020.
- [5] R. Benenson, S. Popov, and V. Ferrari. Large-scale interactive object segmentation with human annotators. In *CVPR*, 2019.
- [6] S. Boyd and L. Vandenberghe. *Convex optimization*. Cambridge university press, 2004.
- [7] A. Chattopadhyay, A. Sarkar, P. Howlader, and V. N. Balasubramanian. Grad-cam++: Generalized gradient-based visual explanations for deep convolutional networks. In *WACV*, 2018.
- [8] J. Choe, S. J. Oh, S. Lee, S. Chun, Z. Akata, and H. Shim. Evaluating weakly supervised object localization methods right. In *CVPR*, 2020.
- [9] J. Choe and H. Shim. Attention-based dropout layer for weakly supervised object localization. In *CVPR*, 2019.
- [10] T. Deselaers, B. Alexe, and V. Ferrari. Weakly supervised localization and learning with generic knowledge. *IJCV*, 100(3):275–293, 2012.
- [11] T. Durand, T. Mordan, N. Thome, and M. Cord. Wildcat: Weakly supervised learning of deep convnets for image classification, pointwise localization and segmentation. In *CVPR*, 2017.
- [12] R. Fu, Q. Hu, X. Dong, Y. Guo, Y. Gao, and B. Li. Axiom-based grad-cam: Towards accurate visualization and explanation of cnns. *BMVC*, 2020.
- [13] W. Gao, F. Wan, X. Pan, Z. Peng, Q. Tian, Z. Han, B. Zhou, and Q. Ye. TS-CAM: token semantic coupled attention map for weakly supervised object localization. *CoRR*, abs/2103.14862, 2021.
- [14] K. He, X. Zhang, S. Ren, and J. Sun. Deep residual learning for image recognition. In *CVPR*, 2016.
- [15] P. Jiang, C. Zhang, Q. Hou, M. Cheng, and Y. Wei. Layercam: Exploring hierarchical class activation maps for localization. *IEEE Trans. Image Process.*, 30:5875–5888, 2021.
- [16] H. Kervadec, J. Dolz, J. Yuan, C. Desrosiers, E. Granger, and I. Ben Ayed. Constrained deep networks: Lagrangian optimization via log-barrier extensions. *CoRR*, abs/1904.04205, 2019.
- [17] M. Ki, Y. Uh, W. Lee, and H. Byun. In-sample contrastive learning and consistent attention for weakly supervised object localization. In *ACCV*, 2020.
- [18] J. Lee, E. Kim, S. Lee, J. Lee, and S. Yoon. Ficklenet: Weakly and semi-supervised semantic image segmentation using stochastic inference. In *CVPR*, 2019.
- [19] M. Lin, Q. Chen, and S. Yan. Network in network. *CoRR*, abs/1312.4400, 2013.
- [20] W. Lu, X. Jia, W. Xie, L. Shen, Y. Zhou, and J. Duan. Geometry constrained weakly supervised object localization. In *ECCV*, 2020.
- [21] J. Mai, M. Yang, and W. Luo. Erasing integrated learning: A simple yet effective approach for weakly supervised object localization. In *CVPR*, June 2020.
- [22] A. Meethal, M. Pedersoli, S. Belharbi, and E. Granger. Convolutional STN for weakly supervised object localization. In *ICPR*, 2020.
- [23] R. Naidu, A. Ghosh, Y. Maurya, S. R. N. K., and S. S. Kundu. IS-CAM: integrated score-cam for axiomatic-based explanations. *CoRR*, abs/2010.03023, 2020.
- [24] R. Naidu and J. Michael. SS-CAM: smoothed score-cam for sharper visual feature localization. *CoRR*, abs/2006.14255, 2020.
- [25] D. Omeiza, S. Speakman, C. Cintas, and K. Weldemariam. Smooth grad-cam++: An enhanced inference level visualization technique for deep convolutional neural network models. *CoRR*, abs/1908.01224, 2019.
- [26] N. Otsu. A threshold selection method from gray-level histograms. *IEEE Transactions on Systems, Man, and Cybernetics*, 9(1):62–66, 1979.
- [27] D. Pathak, P. Krahenbuhl, and T. Darrell. Constrained convolutional neural networks for weakly supervised segmentation. In *ICCV*, 2015.
- [28] P. H. O. Pinheiro and R. Collobert. From image-level to pixel-level labeling with convolutional networks. In *CVPR*, 2015.
- [29] A. Rahimi, A. Shaban, T. Ajanthan, R. Hartley, and B. Boots. Pairwise similarity knowledge transfer for weakly supervised object localization. In *ECCV*, 2020.
- [30] O. Ronneberger, P. Fischer, and T. Brox. U-net: Convolutional networks for biomedical image segmentation. In *MICCAI*, 2015.
- [31] J. Rony, S. Belharbi, J. Dolz, I. Ben Ayed, L. McCaffrey, and E. Granger. Deep weakly-supervised learning methods for classification and localization in histology images: a survey. *CoRR*, abs/1909.03354, 2019.
- [32] R. R. Selvaraju, M. Cogswell, A. Das, R. Vedantam, D. Parikh, and D. Batra. Grad-cam: Visual explanations from deep networks via gradient-based localization. In *ICCV*, 2017.
- [33] K. Simonyan and A. Zisserman. Very deep convolutional networks for large-scale image recognition. In Y. Bengio and Y. LeCun, editors, *ICLR*, 2015.
- [34] K. Singh and Y. Lee. Hide-and-seek: Forcing a network to be meticulous for weakly-supervised object and action localization. In *ICCV*, 2017.
- [35] H. Song, M. Kim, D. Park, and J. Lee. Learning from noisy labels with deep neural networks: A survey. *CoRR*, abs/2007.08199, 2020.
- [36] N. Srivastava, G. Hinton, A. Krizhevsky, I. Sutskever, and R. Salakhutdinov. Dropout: a simple way to prevent neural networks from overfitting. *JMLR*, 15(1):1929–1958, 2014.
- [37] C. Szegedy, V. Vanhoucke, S. Ioffe, J. Shlens, and Z. Wojna. Rethinking the inception architecture for computer vision. In *CVPR*, 2016.
- [38] M. Tang, F. Perazzi, A. Djelouah, I. Ben Ayed, C. Schroers, and Y. Boykov. On regularized losses for weakly-supervised cnn segmentation. In *ECCV*, 2018.
- [39] H. Touvron, M. Cord, M. Douze, F. Massa, A. Sablayrolles, and H. Jégou. Training data-efficient image transformers & distillation through attention. In *ICML*, 2021.
- [40] D. Ulyanov, A. Vedaldi, and V. Lempitsky. Deep image prior. *IJCV*, 128(7):1867–1888, 2020.
- [41] C. Wah, S. Branson, P. Welinder, P. Perona, and S. Belongie. The Caltech-UCSD Birds-200-2011 Dataset. Technical report, California Institute of Technology, 2011.
- [42] F. Wan, P. Wei, Z. Han, J. Jiao, and Q. Ye. Min-entropy latent model for weakly supervised object detection. *PAMI*, 41(10):2395–2409, 2019.

- [43] H. Wang, Z. Wang, M. Du, F. Yang, Z. Zhang, S. Ding, P. Mardziel, and X. Hu. Score-cam: Score-weighted visual explanations for convolutional neural networks. In *CVPR workshop*, 2020.
- [44] J. Wei, Q. Wang, Z. Li, S. Wang, S. K. Zhou, and S. Cui. Shallow feature matters for weakly supervised object localization. In *CVPR*, 2021.
- [45] Y. Wei, J. Feng, X. Liang, M. Cheng, Y. Zhao, and S. Yan. Object region mining with adversarial erasing: A simple classification to semantic segmentation approach. In *CVPR*, 2017.
- [46] Y. Wei, H. Xiao, H. Shi, Z. Jie, J. Feng, and T. S. Huang. Revisiting dilated convolution: A simple approach for weakly- and semi-supervised semantic segmentation. In *CVPR*, 2018.
- [47] H. Xue, C. Liu, F. Wan, J. Jiao, X. Ji, and Q. Ye. Danet: Divergent activation for weakly supervised object localization. In *ICCV*, 2019.
- [48] S. Yang, Y. Kim, Y. Kim, and C. Kim. Combinational class activation maps for weakly supervised object localization. In *WACV*, 2020.
- [49] S. Yang, Y. Kim, Y. Kim, and C. Kim. Combinational class activation maps for weakly supervised object localization. In *WACV*, 2020.
- [50] F. Yu, V. Koltun, and T. Funkhouser. Dilated residual networks. In *CVPR*, 2017.
- [51] S. Yun, D. Han, S. Chun, S. Oh, Y. Yoo, and J. Choe. Cutmix: Regularization strategy to train strong classifiers with localizable features. In *ICCV*, 2019.
- [52] C. Zhang, Y. Cao, and J. Wu. Rethinking the route towards weakly supervised object localization. In *CVPR*, 2020.
- [53] X. Zhang, Y. Wei, J. Feng, Y. Yang, and T. Huang. Adversarial complementary learning for weakly supervised object localization. In *CVPR*, 2018.
- [54] X. Zhang, Y. Wei, G. Kang, Y. Yang, and T. Huang. Self-produced guidance for weakly-supervised object localization. In *ECCV*, 2018.
- [55] X. Zhang, Y. Wei, and Y. Yang. Inter-image communication for weakly supervised localization. In A. Vedaldi, H. Bischof, T. Brox, and J. Frahm, editors, *ECCV*, Lecture Notes in Computer Science, 2020.
- [56] X. Zhang, Y. Wei, Y. Yang, and F. Wu. Rethinking localization map: Towards accurate object perception with self-enhancement maps. *CoRR*, abs/2006.05220, 2020.
- [57] B. Zhou, A. Khosla, A. Lapedrizza, A. Oliva, and A. Torralba. Learning deep features for discriminative localization. In *CVPR*, 2016.
- [58] Z.-H. Zhou. A brief introduction to weakly supervised learning. *National Science Review*, 5(1):44–53, 2017.